GEOLOGY | THE GEOLOGICAL SOCIETY OF AMERICA®

https://doi.org/10.1130/G45589.1

Manuscript received 9 July 2018
Revised manuscript received 13 September 2018
Manuscript accepted 9 January 2019

Tipping the balance: Shifts in sediment production in an active rift setting

Sofia Pechlivanidou[1], Patience A. Cowie[1], Guillaume Duclaux[2], Casey W. Nixon[1], Robert L. Gawthorpe[1], and Tristan Salles[3]

[1]Department of Earth Science, University of Bergen, N-5020 Bergen, Norway
[2]Géoazur, Université Côte d'Azur, CNRS, OCA, IRD, 06560 Valbonne, France
[3]School of Geosciences, University of Sydney, Sydney, 2006 NSW, Australia

ABSTRACT

Landscapes in actively developing rifts respond to tectonic forcing over a similar time scale to that of fault array evolution (i.e., 10^5–10^6 yr). Consequently transient landscapes (i.e., not in topographic steady state) predominate, characterized by focused incision along extensional fault scarps and regional tectonic tilting of surface slopes across strike. Using a field-calibrated numerical model to explore the controls on landscape evolution across the Corinth rift, central Greece, we demonstrate that this tilting, although subtle, leads to a shift in dominant source area as well as a shift toward sediment-starved conditions within the basin. We show, by comparing model runs with and without imposing tectonic forcing, that the impact of active faulting on relief development along the most active Corinth rift margin locally increases erosion rates and footwall incision. However, the overall sediment flux from this margin is reduced because back-tilting lowers erosion rates in catchment headwaters. Conversely, the hanging-wall side of the rift, as it is downwarped, supplies relatively more sediment as rift-directed channel slopes increase even though the relief is decreasing. In summary, we show that tilting plays a key role in controlling the syn-rift sediment flux and, in a counterintuitive way, modifies the relationship between topographic relief and catchment-averaged erosion rates. Our results provide a new perspective on the origin and timing of sediment starvation relative to structural development in rifts.

INTRODUCTION

Source-to-sink studies in rifts focus heavily on patterns of vertical motion along active normal faults (e.g., Cowie et al., 2000; Gawthorpe and Leeder, 2000). Normal faulting not only increases maximum footwall relief and creates hanging-wall accommodation, but also commonly controls sediment entry points along the rift margin. In contrast, the flexural response to active normal faulting leads to differential uplift and/or subsidence, i.e., tilting, as a function of distance away from rift margins regardless of whether high- or low-angle normal faults form (Bell et al., 2017). Hence, large areas of catchments may undergo changes in slope as part of the transient landscape response to active faulting (e.g., Cowie et al., 2006). Any resulting variation in sediment production in space or time affects the facies architecture of the syn-rift fill as well as the potential for feedback between surface mass transfer and tectonics and therefore the structural evolution of the rift (e.g., Maniatis et al., 2009).

Here we perform a surface-process modeling experiment using a natural example of a transient landscape, the Corinth rift, central Greece, where a wealth of published observations of the entire source-to-sink system allows us to explore the impact of observed tectonic forcing on sediment flux. Previous modeling studies of idealized transient landscapes (e.g., Attal et al., 2008) show that over long time scales (~10^6 yr), tilting can lead to drainage-divide migration in extensional settings, but do not consider the impact on relief. By using Corinth as a test case, and focusing on a time scale over which drainage divide migration is minimal (~10^5 yr), we are able to address the following question: If tilting is as important as footwall uplift for relief development along rift margins, what are the consequences for sediment production and ultimately for rift-basin evolution?

STUDY AREA AND METHODS

The Corinth rift in central Greece initiated at ca. 5 Ma and cuts across the preexisting Hellenide fold-and-thrust belt (Leeder et al., 2008). Progressive growth and linkage of normal faults and northward migration of fault activity has resulted in the formation of an east-west–striking asymmetric marine half-graben, ~120 km long and up to 30 km wide (i.e., the Gulf of Corinth; Fig. 1). The syn-rift deformation has been the focus of numerous onshore and offshore studies (e.g., Bell et al., 2009; Roberts et al., 2009), which demonstrate progressive localization of deformation during the Quaternary onto major north-dipping faults bounding the southern rift margin.

We use the surface-processes model pyBadlands (Salles et al., 2018) to simulate landscape development and basin stratigraphy within the Corinth rift. The model integrates hillslope diffusion and river incision by means of a modified stream power law, allowing for balanced sediment transport and deposition under varying tectonic and climatic forcings. We calibrate our model using data for the last 130 k.y. of rift evolution. For this time period, the history of the basin is particularly well constrained. We use published Quaternary uplift and subsidence rates (Table DR2 and Fig. DR1 in the GSA Data Repository[1]) and fault geometry data (Nixon et al., 2016; Bell et al., 2017) to derive the three-dimensional spatial distribution of uplift and subsidence rates that are imposed

[1]GSA Data Repository item 2019094, Table DR1 (model input), Table DR2 (uplift/subsidence rates), Table DR3 (model calibration and sensitivity tests), Table DR4 (erosion rate data), Figure DR1 (displacement map), Figure DR2 (bedrock erodibility), and Figure DR3 (erosion rate analysis), is available online at http://www.geosociety.org/datarepository/2019/, or on request from editing@geosociety.org.

CITATION: Pechlivanidou, S., et al., 2019, Tipping the balance: Shifts in sediment production in an active rift setting: Geology, https://doi.org/10.1130/G45589.1

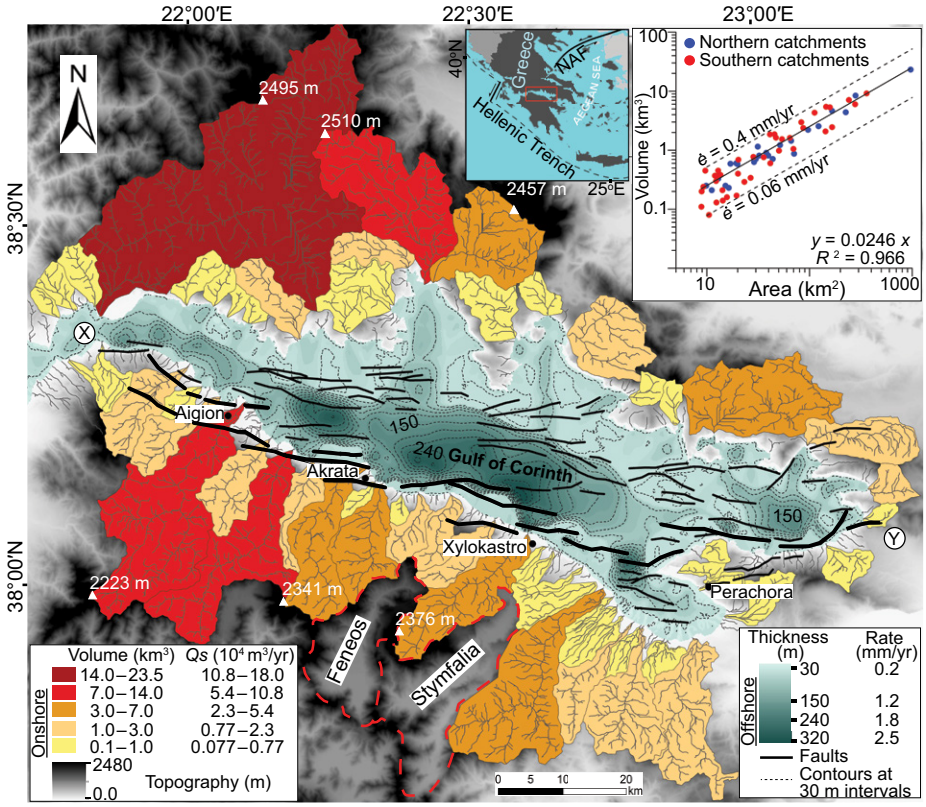

Figure 1. Map view of Corinth rift (central Greece) showing onshore volume removed (warm colors) and offshore volume deposited (cold colors) over the 130 k.y. model run overlain on present-day topography (gray colors). Q_s is the time-averaged sediment flux. Black lines are active faults for this time period from Nixon et al. (2016). Red dashed lines show internally drained areas Feneos and Stymfalia. X and Y indicate end points of profiles in Figure 2. Inset: Sediment volume versus area for northern (blue) and southern (red) catchments (regression line equates to an erosion rate $\dot{e}$ = 0.19 mm/yr by averaging over 130 k.y.; dashed lines depict range of $\dot{e}$).

uniformly over time. Onshore lithostratigraphic units are grouped based on elevation and slope to generate a bedrock erodibility map (Fig. DR2). We include a global sea-level curve to account for eustatic versus lacustrine fluctuations of the base level, and time-averaged climatic data to simulate spatial variations in mean precipitation. Transported sediment is deposited offshore or in depressions on land according to diffusion (Table DR1). The present-day topography is used as the initial surface in all of our model runs. We calculate time-averaged rates of erosion and sedimentation assuming that 130 k.y. is of sufficient length to average out effects of climatic variability on surface processes but is sufficiently short to capture the transient behavior of the landscape.

Model calibration is based on comparing modeled sediment volumes with those obtained from a published interpretation of offshore seismic reflection data (Nixon et al., 2016). We estimate a total offshore (i.e., depositional) grain volume of ~80 km^3 for the past 130 k.y. from the offshore data, which corresponds to ~120 km^3 of onshore (i.e., eroded) volume after correcting for rock porosity onshore. We neglect dissolution in our model, as the deposited sediments are sands, silts, and clays generated by fluvial erosion of the rift margins (see the Data Repository). Additionally, we use geomorphic measures for the present-day and modeled landscapes plus hillslope gradient and curvature to validate our modeling results. Finally, sensitivity tests for erodibility, precipitation, sea level, and hillslope diffusion were performed to quantify the level of uncertainty in our results (Table DR3).

RESULTS

Modeled sediment volumes imply a time-averaged sediment supply to the rift of ~9.5 × 10^5 m^3/yr over the last 130 k.y. (Fig. 1). This value is in close agreement with the sediment volume inferred from the offshore data (i.e., 120 km^3 / 130 k.y. = 9.2 × 10^5 m^3/yr) (see the Data Repository). Furthermore, the modeled offshore depositional pattern is comparable to the results of Nixon et al. (2016) showing depocenters in the central part of the Gulf of Corinth that depict maximum sedimentation rates of ~2.5 mm/yr in the immediate hanging wall of the most active faults.

Output from our calibrated model (Fig. 1) indicates that over 130 k.y. the time-averaged sediment supply from the southern margin of the rift accounts for roughly only half of the total supply (53%) to the offshore even though active tectonic uplift is concentrated along this margin. There is a strong linear correlation between catchment area and the sediment volume produced (R^2 = 0.966; see inset in Fig. 1), and ~50% of the total drainage area lies along the northern, hanging-wall side of the rift and contributes the remaining 47%. Thus, although the southern-margin faults play an obvious role in controlling asymmetric basin subsidence and offshore depositional patterns (Fig. 1), their role in generating onshore relief and potentially enhancing sediment production is more complex. For example, large catchments (>240 km^2), which supply the greatest amounts of sediment (>5 × 10^4 m^3/yr; Figs. 1 and 2), occur along *both* margins and drain areas of preexisting high topography of the Hellenide orogen in the western part of the rift. In contrast, along the central part of the southern margin (i.e., zone C in Fig. 2), where relative uplift rates are highest ($\dot{u} \approx 2$ mm/yr; Fig. 2A) and catchment-averaged erosion rates are also high ($\dot{e} \geq 0.3$ mm/yr; Fig. 2C), the catchments are generally small (<100 km^2) and contribute relatively little sediment (<1 × 10^4 m^3/yr; Figs. 1 and 2B).

Our model results also show that, along the southern margin, $\dot{e}$ correlates with a combination of $\dot{u}$ and maximum relief (C_{max}, in m) (Figs. 2A and 2D). A multiple regression analysis that takes into account that $\dot{u}$ and C_{max} may also be correlated yields the following relation: $\dot{e} = a\,C_{max} + b\,\dot{u}$, where $a = 1 \times 10^{-4}$ yr^{-1} and $b = 5 \times 10^{-2}$ (R^2 = 0.64). Correlations between $\dot{e}$ and C_{max} and between $\dot{e}$ and $\dot{u}$ are significantly weaker (R^2 = 0.55 and R^2 = 0.32, respectively; see the Data Repository). The largest sediment input from the southern margin is from catchments in zone B where $\dot{u}$ is moderately large, C_{max} is high, and catchment areas are relatively large (240–360 km^2). A similar-sized catchment in zone D (southern margin), which drains an area where both $\dot{u}$ and C_{max} are lower, produces less sediment in spite of the presence of highly erodible lithologies (Fig.2E). Clearly $\dot{u}$ and C_{max} together play a more important role in controlling erosion rates along this margin than lithologic variations.

Along the northern margin we find that $\dot{e}$ is, on average, similar to that of the tectonically active southern margin (~0.2 mm/yr; Fig. 1 inset) even though the northern margin is subsiding and contains few, relatively inactive normal faults (Fig. 2A). Furthermore, lower-erodibility lithologies predominate: on average, bedrock erodibility coefficient, K_b, is approximately 1.4× lower than along the southern margin. Unlike along the southern margin, there is no correlation between $\dot{e}$ and C_{max} (Fig. 2D) even though C_{max} varies by ~2000 m (R^2 = 0.23). This combination of factors (subsidence rather than uplift, lower erodibility, lack of correlation between

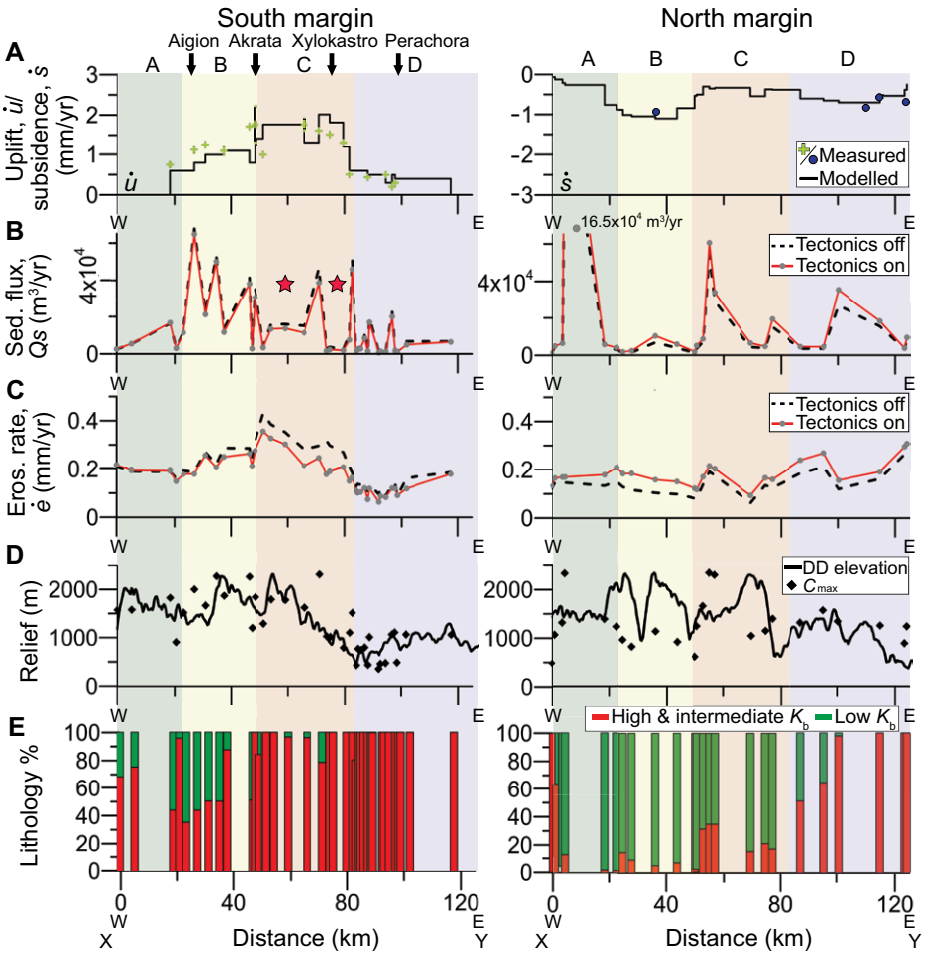

Figure 2. West-to-east along-strike profiles showing modeling results over the 130 k.y. run for each catchment along the southern and northern margins of the Corinth rift (central Greece; see X and Y in Fig. 1; values are projected onto the same west-to-east profile for all catchments). A: Uplift rate, $\dot{u}$, and subsidence rate, $\dot{s}$, at catchment mouth. Measured uplift and subsidence rates are shown with green crosses and blue dots, respectively (see Fig. DR1 [see footnote 1]). Black arrows at top depict localities shown in Figure 1. B: Time-averaged sediment flux, Q_s. C: Catchment-averaged erosion rate, $\dot{e}$. Red stars depict location of drainage reversals (i.e., Feneos and Stymfalia; see Fig. 1). Black dashed lines in B and C show modeling results for runs without imposed tectonic forcing (see Fig. 3). D: Maximum catchment relief, C_{max}. Thick black lines show elevation of main drainage divide (DD). E: Percentage of high- and intermediate- versus low-erodibility (K_b) lithologies. Zones A, B, C, and D are defined by uplift patterns along the southern margin.

$\dot{e}$ and C_{max}) favors lower catchment-averaged erosion rates so that the northern margin might be expected to contribute significantly less than the southern margin. However, our results demonstrate that this not the case (Figs. 1 and 2).

Via a simple experiment, we demonstrate what leads to the unexpectedly high erosion rates along the northern margin by comparing our calibrated model results to a model in which we do not impose tectonic forcing (Figs. 2 and 3). Figure 3 shows the difference in time-averaged erosion rate for these two cases, with our calculation steps explicitly shown for one footwall catchment in Figures 3B–3D. When tectonic forcing is imposed, there is an overall decrease in erosion rates along the southern margin relative to the run without tectonic forcing (Figs. 2C and 3) even though uplift increases the maximum relief along this margin by ~8% on average. Footwall uplift leads to local river incision close to the active faults (Figs. 3A and 3B), and some areas with high erosion rates upstream are related to preexisting relief (Fig. 3C). However, over most of the upper reaches, erosion rates are lower because of back-tilting. In contrast, catchments lying on the northern, hanging-wall side of the rift show a positive difference in erosion rates between the two model runs, implying higher erosion rates in the run where tectonics is switched on (Figs. 2C and 3), in spite of the fact that the maximum relief along the northern margin is lower in this case (~3.5% on average) because of tectonic subsidence. Subsidence reduces the contributing area by ~13% because of shoreline changes, but the enhanced erosion rate that results from tilting toward the rift is the dominant effect. Between the two runs, the relative contribution of the southern versus northern margins changes from 60:40 to 53:47 when tectonic forcing is imposed.

The long-term effect of back-tilting along the southern margin is that headwater areas become vulnerable to capture or drainage reversal so that, over longer time scales, the contributing area and thus *total* sediment supplied to the rift can drop (cf. Attal et al., 2008). For example, we infer that the *total* sediment supply dropped by ~1.15×10^5 m^3/yr (estimate based on the area-volume relationship shown in Fig. 1 inset) when the areas of Stymfalia and Feneos (Fig. 1) became internally drained at ca. 800 ka (Gawthorpe et al., 2018; see Fig. 1, and red stars in Fig. 2B). Importantly, such drainage reversals further increase the *relative* contribution of the northern margin.

CONCLUSIONS AND IMPLICATIONS

Our experiment, based on the transient landscape evolution of the Corinth rift, demonstrates how tilt-induced changes in slope at the fault-block scale modify the topographic relief of sediment source areas. Significantly, as a consequence of the tilting, the correlation between maximum topographic relief and catchment-averaged erosion rates collapses, most obviously along the hanging-wall (northern) margin but also along the footwall (southern) margin. Sediment flux is thus not necessarily enhanced when normal faulting increases maximum catchment relief (cf. Syvitski and Milliman, 2007). The sediment flux from footwall catchments can in fact decrease as preexisting topographic relief and antecedent drainage networks are back-tilted, resulting in lower erosion rates in catchment headwaters (Fig. 3). Conversely, tilting (or downwarping) of the hanging wall, caused by localized slip along the southern-margin faults, can increase the sediment flux from the northern margin. This increase occurs because fluvial channels on the hanging-wall margin become steeper even though the region is subsiding and maximum relief is decreasing. Together, tilting along the two rift margins results in a "shift" such that the northern, less active margin becomes an increasingly important source area even though the southern-margin faults are the main control on depocenter development.

Our results lead to a reevaluation of cause and effect with respect to a key feature of rifts. Given the typical ratio of footwall uplift to hanging-wall subsidence on normal faults (e.g., in Corinth, 1:1.2–2.2; McNeill and Collier, 2004), hanging-wall basins are expected to be relatively undersupplied with sediment during the onset of extension. However, in many rifts, extensive fluvial deposition characterizes the earliest stages of extension, highlighting the importance of an initial sediment supply that derives from preexisting sediment source areas.

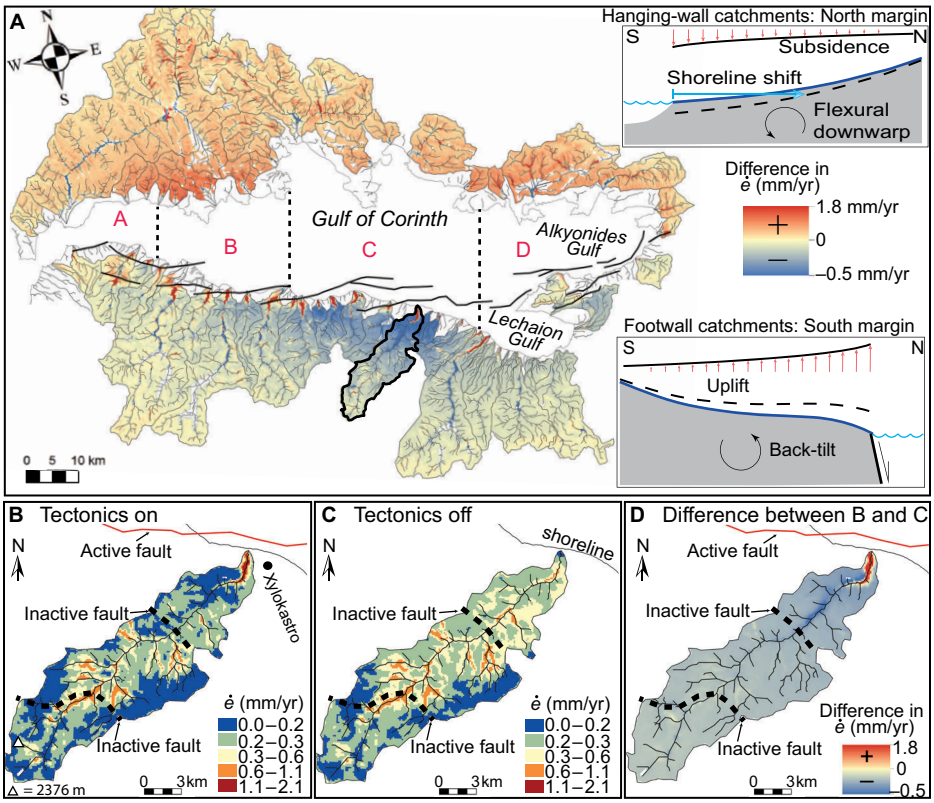

Figure 3. A: Difference in erosion rates, *ė*, between model runs with and without imposed tectonic forcing for all catchments draining into Gulf of Corinth. Black dashed lines depict the four zones (A, B, C, and D) described in Figure 2. Upper inset illustrates impact of flexural downwarp for catchments lying along northern rift margin (i.e., hanging-wall catchments), and lower inset illustrates impact of back-tilt for catchments lying along southern rift margin (i.e., footwall catchments). B,C: Spatial variation in *ė* with and without imposing tectonic forcing, respectively, for catchment outlined in black in A. D: Difference in *ė* between the two model runs.

As back-tilting along footwall-controlled margins may be sufficient to cause a reduction in this supply, a transition from oversupplied to sediment-starved conditions may emerge spontaneously during the extension history and may not require any increase in tectonic subsidence rate to be explained (cf. Gupta et al., 1998). Furthermore, if the drop in sediment supply precedes the increase in tectonic subsidence rate, the feedback between surface mass transfer and normal faulting may not be the main causal factor for increased rates of fault slip during rift evolution (cf. Maniatis et al., 2009).

ACKNOWLEDGEMENTS

We acknowledge funding from Research Council of Norway (project 255229/E30) and industry partners: Aker BP, ConocoPhillips, Faroe Petroleum, Equinor, Tullow Oil, and VNG Norge. R.L. Gawthorpe acknowledges support from VISTA Equinor and the Norwegian Academy of Science and Letters. We thank R. Cox and two anonymous reviewers for their helpful comments. The University of Bergen is acknowledged for supporting Open Access publication.

REFERENCES CITED

Attal, M., Tucker, G.E., Whittaker, A.C., Cowie, P.A., and Roberts, G.P., 2008, Modeling fluvial incision and transient landscape evolution: Influence of dynamic channel adjustment: Journal of Geophysical Research, v. 113, F03013, https://doi.org/10.1029/2007JF000893.

Bell, R.E., McNeill, L.C., Bull, J.M., Henstock, T.J., Collier, R.E.L., and Leeder, M.R., 2009, Fault architecture, basin structure and evolution of the Gulf of Corinth Rift, central Greece: Basin Research, v. 21, p. 824–855, https://doi.org/10.1111/j.1365-2117.2009.00401.x.

Bell, R.E., Duclaux, G., Nixon, C.W., Gawthorpe, R.L., and McNeill, L.C., 2017, High-angle, not low-angle, normal faults dominate early rift extension in the Corinth Rift, central Greece: Geology, v. 46, p. 115–118, https://doi.org/10.1130/G39560.1.

Cowie, P.A., Gupta, S., and Dawers, N.H., 2000, Implications of fault array evolution for synrift depocentre development: Insights from a numerical fault growth model: Basin Research, v. 12, p. 241–261, https://doi.org/10.1111/j.1365-2117.2000.00126.x.

Cowie, P.A., Attal, M., Tucker, G.E., Whittaker, A.C., Naylor, M., Ganas, A., and Roberts, G.P., 2006, Investigating the surface process response to fault interaction and linkage using a numerical modelling approach: Basin Research, v. 18, p. 231–266, https://doi.org/10.1111/j.1365-2117.2006.00298.x.

Gawthorpe, R.L., and Leeder, M.R., 2000, Tectono-sedimentary evolution of active extensional basins: Basin Research, v. 12, p. 195–218, https://doi.org/10.1046/j.1365-2117.2000.00121.x.

Gawthorpe, R.L., Leeder, M.R., Kranis, H., Skourtsos, E., Andrews, J.E., Henstra, G.A., Mack, G.H., Muravchik, M., Turner, J.A., and Stamatakis, M., 2018, Tectono-sedimentary evolution of the Plio-Pleistocene Corinth rift, Greece: Basin Research, v. 30, p. 448–479, https://doi.org/10.1111/bre.12260.

Gupta, S., Cowie, P.A., Dawers, N.H., and Underhill, J.R., 1998, A mechanism to explain rift-basin subsidence and stratigraphic patterns through fault-array evolution: Geology, v. 26, p. 595–598, https://doi.org/10.1130/0091-7613(1998)026<0595:AMTERB>2.3.CO;2.

Leeder, M.R., Mack, G.H., Brasier, A.T., Parrish, R.R., McIntosh, W.C., Andrews, J.E., and Duermeijer, C.E., 2008, Late-Pliocene timing of Corinth (Greece) rift-margin fault migration: Earth and Planetary Science Letters, v. 274, p. 132–141, https://doi.org/10.1016/j.epsl.2008.07.006.

Maniatis, G., Kurfeß, D., Hampel, A., and Heidbach, O., 2009, Slip acceleration on normal faults due to erosion and sedimentation—Results from a new three-dimensional numerical model coupling tectonics and landscape evolution: Earth and Planetary Science Letters, v. 284, p. 570–582, https://doi.org/10.1016/j.epsl.2009.05.024.

McNeill, L.C., and Collier, R.E.L., 2004, Uplift and slip rates of the eastern Eliki fault segment, Gulf of Corinth, Greece, inferred from Holocene and Pleistocene terraces: Journal of the Geological Society, v. 161, p. 81–92, https://doi.org/10.1144/0016-764903-029.

Nixon, C.W., et al., 2016, Rapid spatiotemporal variations in rift structure during development of the Corinth Rift, central Greece: Tectonics, v. 35, p. 1225–1248, https://doi.org/10.1002/2015TC004026.

Roberts, G.P., Houghton, S.L., Underwood, C., Papanikolaou, I., Cowie, P.A., van Calsteren, P., Wigley, T., Cooper, F.J., and McArthur, J.M., 2009, Localization of Quaternary slip rates in an active rift in 10^5 years: An example from central Greece constrained by ^{234}U-^{230}Th coral dates from uplifted paleoshorelines: Journal of Geophysical Research, v. 114, B10406, https://doi.org/10.1029/2008JB005818.

Salles, T., Ding, X., and Brocard, G., 2018, pyBadlands: A framework to simulate sediment transport, landscape dynamics and basin stratigraphic evolution through space and time: PLoS One, v. 13, e0195557, https://doi.org/10.1371/journal.pone.0195557.

Syvitski, J.P.M., and Milliman, J.D., 2007, Geology, geography, and humans battle for dominance over the delivery of fluvial sediment to the coastal ocean: Journal of Geology, v. 115, p. 1–19, https://doi.org/10.1086/509246.

Printed in USA